



Cite this: *J. Mater. Chem. A*, 2021, 9, 1025

Novel composite hydrogels containing fractionated, purified lignins for aqueous-based separations†

Nicholas Gregorich,  Junhuan Ding, Mark C. Thies and Eric M. Davis *

Herein, a series of novel, lignin-based hydrogel composites was fabricated by incorporating ultraclean lignins (UCLs), of controlled molecular weight and low dispersity, into poly(vinyl alcohol) (PVA). The UCLs were obtained from a novel liquid–liquid fractionation of high dispersity crude bulk lignins (CBLs) obtained from Kraft black liquor. A complementary series of composite hydrogels was fabricated using these CBLs. Both the CBLs and UCLs were functionalized with vinyl-containing acrylate groups allowing the lignins to chemically crosslink with themselves, forming an interpenetrated network with the thermally-crosslinked network of PVA chains. Successful functionalization of the UCLs was demonstrated by proton and phosphorous nuclear magnetic resonance. PVA–lignin hydrogels containing 20 wt% UCL saw a reduction in methylene blue (MB) permeability by approximately two orders of magnitude when compared to neat PVA. Further, for composite hydrogels containing either 50 wt% UCL or CBL, no MB was detected in the receiving reservoir over the duration of the permeation experiment. In general, an increase in Young's moduli was observed in PVA–lignin hydrogels containing CBLs, where hydrogels composed of 50 wt% CBLs exhibited ~40% increase when compared to neat PVA. In contrast, a ~10% reduction in Young's moduli was observed for composite hydrogels containing 20 wt% UCLs or less, though these membranes exhibited the lowest MB permeabilities of all membranes investigated. However, the largest increase in membrane stiffness was observed for composite hydrogels containing 50 wt% UCLs, where a ~70% increase in Young's modulus was observed. Finally, the concentration and functionalization of the lignins was seen to have a direct impact on the network structure of the soft composites, where in general, the molecular weight between crosslinks is seen to decrease with increasing lignin concentration.

Received 14th September 2020
Accepted 25th November 2020

DOI: 10.1039/d0ta09046h

rsc.li/materials-a

1. Introduction

Hydrogels are attractive materials for aqueous-based separations as the selectivity of the membrane can be directly influenced through manipulation of its network structure (*i.e.*, mesh size) and chemical composition (or functionality). As such, these soft materials have been used to separate oil from water/oil emulsions,¹ organic dyes (*e.g.*, methylene blue)^{2,3} and heavy metal ions (*e.g.*, Cu²⁺, Pb²⁺) from aqueous solutions,^{4,5} as well as controlled adsorption and release of model drugs⁶ and model proteins, such as bovine serum albumin.^{7–9} However, the use of petroleum-based precursors in the fabrication of traditional synthetic hydrogels – *e.g.*, poly(acrylic acid), poly(acrylamide), poly(vinyl alcohol) – has resulted in increased interest in the use of environmentally friendly, renewable biopolymers for these membrane-based separations. As such, the use of renewable

biopolymers, such as chitosan,^{7,8,10} cellulose,^{11,12} and lignin,^{3,13–27} in the fabrication of next-generation materials has been extensively researched.

Of particular interest to the current work is the use of lignin in the fabrication of soft composites. As an additive for composite hydrogels, lignin possesses several beneficial attributes, including antioxidant^{28,29} and antimicrobial properties,^{30,31} high ultra-violet (UV) light absorption,^{32,33} and high thermal stability.³⁴ In addition, the abundance of hydroxyl (–OH) groups and chemical linkages allow for the potential of a wide variety of chemical functionalizations,³⁵ although access to these groups is not straightforward due to the complex and heterogeneous structure of the lignins.^{34,36,37} Lastly, as lignin is the world's second most abundant natural polymer (behind only cellulose),^{34,38–40} lignin-based composite membranes present an opportunity to substantially reduce the use of petroleum-based products.^{41,42}

Lignin holds significant potential for added value in the fabrication of advanced soft composites,^{43,44} with ~50 million tons per year readily available as a by-product of biomass processing. However, today, >99% of that lignin is simply burned as

Department of Chemical and Biological Engineering, Clemson University, Clemson, SC 29634, USA. E-mail: ericd@clemson.edu

† Electronic supplementary information (ESI) available. See DOI: 10.1039/d0ta09046h

fuel or sent to waste treatment.⁴⁵ Approximately 90% of the lignin that is recovered (~150 000 tons) is Kraft lignin from pulp mills,^{34,45} and is used in materials applications. However, all of the recovery methods in use today indiscriminately precipitate and isolate crude bulk lignins (CBLs), which have broad molecular weight (MW) distributions (*i.e.* high dispersity (\mathcal{D})), complex and heterogeneous chemical architectures, and low purities.³⁴ Furthermore, the recovered CBLs possess a high metals content (~10 000 ppm total metals, primarily sodium and potassium), which is of particular concern for bioseparations,⁴⁵ as metals can leach out of the composite material into the human body or into an expensive product stream, presenting risks for both health and product contamination. Note, lignin can be further broken down into small molecule, oligomeric products, through processes such as catalytic depolymerization^{46–48} or pyrolysis.^{49–51} However, use of such materials was not the focus of the current study, as these methods completely destroy the unique polymeric nature of lignin.⁵²

The addition of lignin to hydrogels has been demonstrated as a viable means of altering both the mechanical and permselective properties of composite lignin hydrogels.^{20–22,28,34,35,53–55} However, starting with early work in the late 1970s and early 1980s by Lindström and Westman,^{56–58} to date, the vast majority of studies regarding lignin-based hydrogels involve fabrication methods that utilize heterogeneous, ill-defined lignins (*i.e.*, CBLs with high \mathcal{D}).^{54,59–81} Furthermore, developing lignin-based hydrogels for targeted separations is hindered by our lack of understanding as to how the addition of lignins to these soft composites alters the crosslinked network structure of the resulting hydrogel. When used in the fabrication of composite hydrogels, the heterogeneity of the lignins results in composites with ill-defined network structures, obfuscating the molecular-scale interactions and fundamental mechanism governing transport in these green materials. Fortunately, recent work by Thies and co-workers^{38,45,82} involving the fractionation and purification of CBLs has presented a feasible avenue for obtaining lignins of well-defined MWs and low \mathcal{D} . Specifically, they have developed the Aqueous Lignin Purification with Hot Agents (ALPHA) process,⁸³ which can be used to continuously and simultaneously clean, fractionate, and solvate lignins into prescribed MWs of narrow dispersity ($\mathcal{D} \approx 2$), having metals contents lower than 50 ppm (referred to as ultraclean lignins (UCLs)).⁴⁵ Incorporating UCLs of prescribed MWs and low dispersity into hydrogels should, in principle, result in a more homogeneous network structure of the composite hydrogel. Moving forward, such materials systems will allow us to more accurately elucidate the fundamental relationships between lignin molecular weight, soft composite network structure, and membrane separation performance for this emerging class of green materials.

Traditionally, poly(vinyl alcohol) (PVA) hydrogels have been synthesized *via* thermal crosslinking,^{84,85} chemical crosslinking,^{86–96} or a combination of both.^{88,97} They have also been synthesized *via* freeze-thaw methods inducing physical crosslinks.^{98–106} In the case of thermal crosslinking, physical crosslinks are formed in the PVA hydrogels through the formation of crystallites. This has proven to be a viable method for creating

free-standing PVA membranes that are stable when re-immersed in water (*i.e.*, they do not redissolve when placed in water). As the crosslinks formed in this case are not permanent crosslinks, thermally-crosslinked PVA films are susceptible to dissolution if placed in water at elevated temperatures (>60 °C). In the case of chemically-crosslinked PVA films, permanent crosslinks between chains are achieved through the use of a crosslinking agent. For example, stable chemical crosslinking of PVA hydrogels has been achieved with glutaraldehyde,^{86–93} and various acids,^{94–96} to name a few. As hydroxyl groups along the backbone of the hydrogel are consumed during the crosslinking process, the resulting membranes are much less hydrophilic than neat PVA. While this can be leveraged as a means to alter the hydrophilicity of the crosslinked membrane, it may also be beneficial to retain the high hydrophilicity of the neat PVA in the resulting membrane, especially for lower temperature applications, where the stability of the PVA membrane is not in question.

In this work, two series of PVA composite hydrogels containing unfunctionalized and functionalized lignins at concentrations ranging from 0 to 50 wt% were synthesized. These soft composites were fabricated using both crude bulk lignins (CBLs; apparent number-average molecular weight, $M_{N,app} \approx 4170 \text{ g mol}^{-1}$, dispersity, $\mathcal{D} \approx 3.9$) that were recovered from a Southeastern pine black liquor *via* the Sequential Liquid-Lignin Recovery and Purification (SLRP) process,¹⁰⁷ and ultraclean lignins (UCLs; apparent number-average molecular weight, $M_{N,app} \approx 1250 \text{ g mol}^{-1}$, dispersity, $\mathcal{D} \approx 2.2$), which were isolated from the aforementioned CBLs *via* the ALPHA process. Detailed descriptions of the SLRP and ALPHA techniques are given elsewhere.⁸² The chemical functionality of the lignins was altered *via* an acrylation process, where a portion of the –OH groups were replaced with vinyl groups (*i.e.*, C=C). This functionalization allows for the formation of an interpenetrated network (IPN)^{108–115} containing chemically-crosslinked lignin and thermally-crosslinked PVA. Successful functionalization of –OH groups was confirmed by both proton and phosphorus nuclear magnetic resonance (¹H NMR and ³¹P NMR, respectively), as well as *via* infrared spectroscopy. The mechanical and transport properties of the soft composites were also measured. Specifically, the Young's moduli of the hydrated composites were characterized using mechanical indentation, while the permeability of methylene blue (MB) across the membranes was captured by ultraviolet-visible (UV-vis) spectroscopy. Note, as a 'proof of concept' regarding the fabrication of composite hydrogels with high lignin content, composite hydrogels containing 50 wt% unfunctionalized CBL and UCL were also fabricated.

2. Results and discussion

2.1. Lignin characterization and composite hydrogel fabrication

The nomenclature for each of the composite hydrogels is summarized in Table 1.

Fig. 1 shows the proposed reaction schemes and an image of free-standing membranes for neat (or pristine) PVA and the two

Table 1 Nomenclature for PVA–lignin composite hydrogels

Type of lignin	Lignin content	Unfunctionalized (UF) or functionalized (F)	Nomenclature
UCLs	10 wt%	UF	PVA–UCL–10UF
		F	PVA–UCL–10F
	20 wt%	UF	PVA–UCL–20UF
		F	PVA–UCL–20F
	50 wt%	UF	PVA–UCL–50UF
		F	PVA–UCL–50F
CBLs	10 wt%	UF	PVA–CBL–10UF
		F	PVA–CBL–10F
	20 wt%	UF	PVA–CBL–20UF
		F	PVA–CBL–20F
	50 wt%	UF	PVA–CBL–50UF
		F	PVA–CBL–50F

series of hydrogel composites synthesized in this work. Specifically, Reaction Schematic No. 1 in Fig. 1a shows the proposed reaction scheme for neat PVA and PVA–lignin composite hydrogels synthesized *via* thermal crosslinking. As previously mentioned, thermal crosslinking is one route by which dense, free-standing PVA hydrogels can be fabricated.^{84,85} In the schematic of the proposed network structure for these neat PVA

hydrogels, the green dots represent the physical crosslinks between PVA chains created during the thermal crosslinking process. In addition to neat PVA hydrogels, Reaction Schematic No. 1 shows the proposed network structure of the thermally-crosslinked PVA–lignin hydrogels, whereby the unfunctionalized lignins (shown as curved blue lines) remain in the hydrogel *via* physical entanglements with the thermally-crosslinked network of PVA chains. Next, Reaction Schematic No. 2 in Fig. 1a shows the proposed reaction scheme for PVA–lignin composite hydrogels synthesized *via* combined thermal and chemical crosslinking with functionalized CBLs and UCLs.^{86–96} In the schematic, the –OH groups on lignin are colored in blue and the reactive vinyl groups, containing a C=C bond that undergoes free radicalization, are colored in red. Prior to synthesis of the composite hydrogel, the CBLs and UCLs are first functionalized, undergoing an acrylation process that replaces some of the –OH groups on lignin with vinyl groups containing a C=C bond, allowing the functionalized lignins to act as an additional crosslinker in the reaction scheme. In the schematic for the proposed network structure of these PVA–lignin hydrogels, the red dots represent the chemical crosslinks between functionalized lignin chains (shown as curved purple

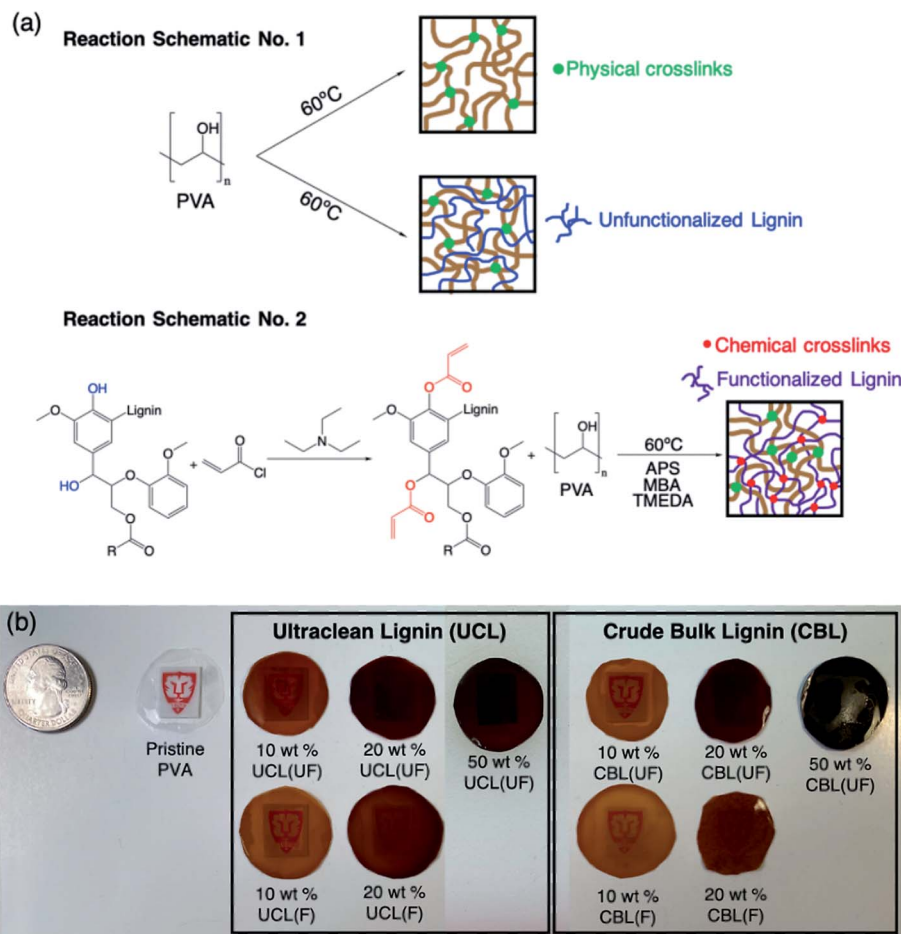


Fig. 1 (a) Reaction schematic and proposed network structure for thermally-crosslinked, as well as thermally- and chemically-crosslinked PVA–lignin composite hydrogels using both unfunctionalized and functionalized lignin. (b) Picture of free-standing neat PVA and PVA–lignin hydrogels containing 0 wt% to 50 wt% unfunctionalized and functionalized UCLs and CBLs.

lines). As shown in the schematic, these composite hydrogels form an IPN of thermally-crosslinked PVA chains and chemically-crosslinked lignin chains.

As seen in Fig. 1b, successful fabrication of stable, free-standing, crosslinked PVA hydrogels *via* both reaction schemes was achieved. Fig. 1b contains an image of the free-standing hydrogel composite membranes with lignin concentrations ranging from 0 wt% (*i.e.*, neat PVA) to 50 wt% CBLs and UCLs. As seen in Fig. 1b, the optical properties of the hydrogels change significantly with the introduction of lignin, with membranes becoming less transparent as the lignin content was increased from 10 wt% to 50 wt%. This lack of transparency is most noticeable for PVA-CBL-50UF, where these membranes are almost completely opaque. Note, as shown in Table S2 in the ESI,[†] all of the membranes were stable in room temperature water ($\sim 20^\circ\text{C}$) for >120 days. Further, all membranes remained stable up to a temperature of 40°C for 4 hours. Above 40°C , for both series of composite hydrogels, the thermal stability of the membranes varied with both functionalization and lignin content. Interestingly, the hydrogels containing unfunctionalized CBL at 20 wt% and 50 wt% remained stable (*i.e.*, did not dissolve or break down) up to temperatures of 80°C for 24 hours. While degradation (or lack thereof) of these membranes at higher temperatures presents an area of interest, full thermal characterization of these membranes is outside the scope of this investigation, as all mechanical and transport properties were characterized for composite membranes at room temperature ($\sim 20^\circ\text{C}$).

To ensure the CBLs and UCLs were properly acrylated, both ^1H and ^{31}P NMR were performed on the lignins before and after functionalization. For the sake of conciseness, only the ^{31}P NMR spectra have been presented in the manuscript (see Fig. S1 in the ESI[†] for ^1H NMR data). Fig. 2a and b show the ^{31}P NMR spectra of the UCLs and CBLs, respectively, before (dashed blue line) and after (solid red line) acrylation. While the use of ^{31}P NMR may not seem intuitive given the lack of phosphorous groups in lignin, phosphorylation of the $-\text{OH}$ groups in lignin, by reagents such as 2-chloro-4,4,5,5-tetramethyl-1,3,2-

dioxaphospholane, is carried out prior to conducting ^{31}P NMR experiments.^{116,117} This process is commonly utilized to quantify the type and amount of hydroxyl groups present in lignins,^{116–120} and was therefore employed in our current work. The broad peak on the left-hand side of each figure is associated with the aliphatic $-\text{OH}$ groups, while the collection of peaks on the right-hand side are associated with the aromatic $-\text{OH}$ groups of the lignins.¹¹⁷ As seen from these two figures, the decrease in height of the NMR spectral peaks indicates that the concentrations of $-\text{OH}$ groups on both the UCLs and CBLs have decreased after the lignins underwent acrylation. This is quantitatively shown in Table S1 of the ESI,[†] where it can be seen that for both the CBLs and UCLs, the $-\text{OH}$ content (mmol OH/g lignin) is lower post functionalization. Further, if we take a deeper look at the $-\text{OH}$ contents pre- and post-functionalization, it is apparent that, collectively, a higher degree of functionalization occurred in the UCLs as compared to CBLs. That is, a higher concentration of $-\text{OH}$ groups were consumed during acrylation. Specifically, post functionalization, an $\sim 60\%$ decrease in the total $-\text{OH}$ content (aliphatic + aromatic) of the UCLs was observed, while only a $\sim 54\%$ decrease was observed for the CBLs. The reactivity difference between these two lignins highlights the lower steric hinderance for the $-\text{OH}$ groups in the ultraclean, fractionated UCLs (*i.e.*, there is better access to the $-\text{OH}$ groups in the UCLs). Interestingly, relative reactivity of the aliphatic and aromatic $-\text{OH}$ groups varied between the CBLs than UCLs, where a higher reactivity of the aromatic $-\text{OH}$ groups was observed for the UCLs. To further verify successful functionalization of the lignins, the addition of the $\text{C}=\text{C}$ bond to the functionalized lignin was confirmed *via* ^1H NMR (see Fig. S1 in the ESI[†]).

2.2. Separation performance of the composite hydrogels

The aqueous-separation properties of the PVA-lignin composite hydrogels were characterized by performing methylene blue (MB) permeability experiments. For these experiments, the hydrogels were challenged with a high concentration of MB on one side of the membrane, and the concentration of permeated MB in the receiving reservoir – *i.e.*, the reservoir on the side of

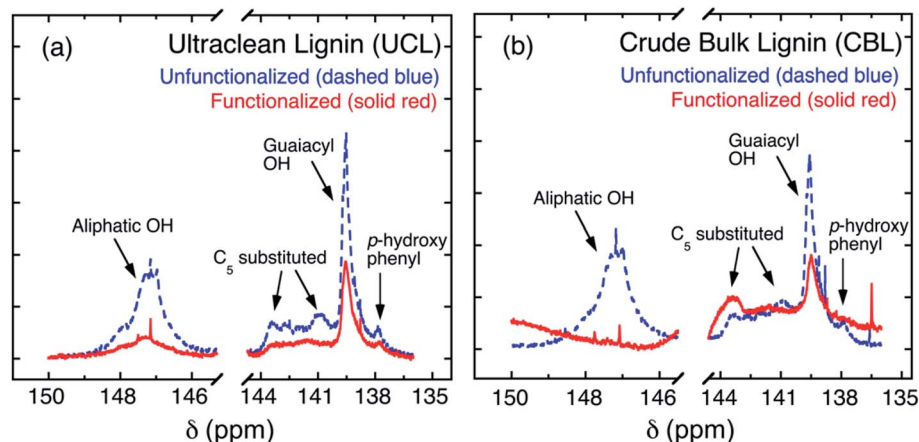


Fig. 2 ^{31}P NMR spectra of unfunctionalized (dashed blue line) and functionalized (solid red line) (a) ultraclean lignins (UCLs) and (b) crude bulk lignins (CBLs).

the membrane opposite the MB solution – was measured as a function of time. Fig. 3a and b show the results of the MB permeation experiments performed on neat PVA, as well as PVA–lignin hydrogel composites containing both unfunctionalized and functionalized UCLs and CBLs, respectively. More specifically, these two figures show the concentration of MB in the receiving reservoir as a function of time. Note, the time data have been normalized by the square of the thicknesses of the hydrogels so direct comparisons between membranes of different thicknesses can be made. Also note that MB permeation data for PVA–UCL–50UF and PVA–CBL–50UF is not shown in Fig. 3, as there was never a detectable concentration of MB in the receiving reservoir. That is, membranes with 50 wt% UCL and CBL adsorbed the entire amount of MB loaded in the donating reservoir. Therefore, no permeation analysis was performed on these membranes. In general, a visual inspection of the slopes of these normalized data provide qualitative insight into the relative changes in the MB permeability, where reductions in MB permeability manifest as reductions in the slopes of these data. Interestingly, as seen in Fig. 3a and b, an

initial ‘lag time’ is observed in the MB permeation data for all PVA–lignin composite hydrogels, where for a period of time, no MB is detected in the receiving reservoir. As this is observed with all lignin-containing composite hydrogels, we believe this initial lag in the permeability data is a direct result of electrostatic interactions between the diffusing MB molecules and the –OH groups of the lignins inside the membranes. In water, MB has a positive charge (*i.e.*, cationic), which results in attractive electrostatic interactions with the –OH groups in lignin.

If we focus our attention on Fig. 3a, this assertion appears to be further validated by the fact that the length of the initial lag is directly affected by both the amount of UCL in the composite membranes, as well as whether or not the UCL had undergone functionalization. With regards to the concentration of lignin, the time before initial MB breakthrough increased significantly as the UCL concentration in the hydrogel composites was increased from 10 wt% to 20 wt%. Further, it can be seen that this initial lag time is longer for composite membranes containing unfunctionalized UCLs. This is most easily seen when comparing PVA–UCL–20UF (open blue circles) to PVA–UCL–20F

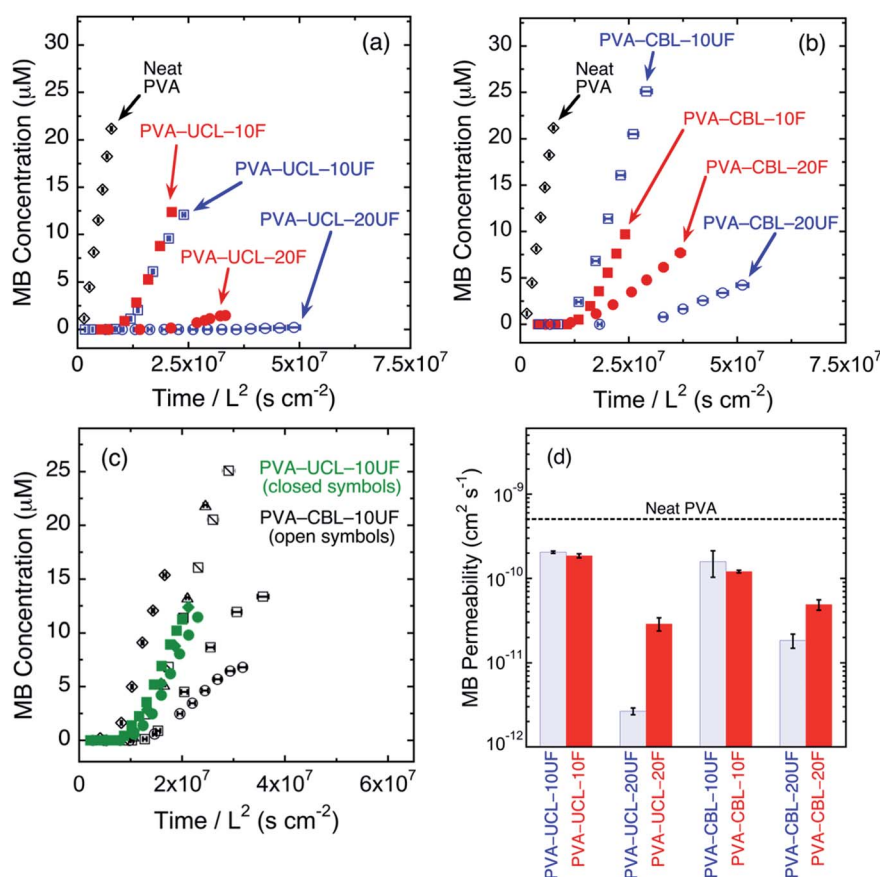


Fig. 3 Concentration of methylene blue (MB) in the receiving cell as a function of time for neat PVA and PVA membranes containing various amounts of unfunctionalized and functionalized (a) ultraclean lignins (UCLs) and (b) crude bulk lignins (CBLs). Note, the data have been normalized by the square of the membrane thickness. (c) Concentration of MB in the receiving cell as a function of time for PVA membranes containing 10 wt% UCLs (closed green symbols) and CBLs (open black symbols), both unfunctionalized. Each data set is a unique MB permeation experiment on an individual hydrogel sample. Note, some of the data displayed in Fig. 3a and b was reshown in 3c, as part of a collection of multiple experiments. (d) Summary of the calculated MB permeabilities for neat PVA and PVA–lignin composite hydrogels. The dashed black line indicates the average MB permeability for neat (or pristine) PVA (*i.e.*, PVA containing no lignin). Note, the error bars in the figure represent the standard deviation of (at least three) repeat experiments.

(closed red circles) in Fig. 3a. The trends in these data follow what we would expect, based on the chemistry involved in the lignin functionalization.

As shown in Fig. 1a (Reaction Schematic No. 2), acrylation of the lignins replaces the $-OH$ groups in the lignins with $C=C$ bonds, ultimately resulting in a lower concentration of $-OH$ groups in the functionalized lignins (see Table S1 in ESI† for quantitative hydroxyl content). The lower hydroxyl content should lead to less electrostatic interactions between the diffusing MB and the functionalized lignins, resulting in longer initial lag times in the data for hydrogels containing unfunctionalized lignin *versus* their functionalized counterpart. This, for the most part, is what we observe in the data for both series of hydrogels containing UCLs and CBLs (open blue circles *vs.* closed red circles in Fig. 3a and b, respectively). For hydrogels containing 10 wt% CBLs, the initial lag times in the data are approximately the same, regardless of lignin functionalization. Interestingly, when we compare the initial lag times for PVA-lignin composites containing unfunctionalized UCLs and CBLs at 20 wt%, we see that the length of time before which MB is detected on the opposite side of membrane is significantly higher for membranes containing unfunctionalized UCLs. This result is worth noting, as it alludes to the possibility that for composite membranes containing unfunctionalized UCLs, a greater concentration of $-OH$ groups are available (or are accessible) to electrostatically interact with the MB as it diffuses through the composite hydrogel.

While the proposed chemical structures of lignin show numerous $-OH$ groups,¹²¹ access to these groups is hindered due to the complex (branched), collapsed structure of the CBLs. Our results appear to indicate that the UCLs have a less collapsed structure (or chemical architecture) inside of the composite hydrogel when compared to the CBLs. That is, the $-OH$ groups in the UCLs are more easily accessible than those in the CBLs, which is more than likely due to the higher steric hindrance of the $-OH$ groups in the higher MW, high dispersity CBLs. The higher concentration of accessible $-OH$ groups on the UCLs can be further suggested by the fact that the length of time before MB is measured on the other side of PVA-UCL-20F composite membranes is similar to that of PVA-CBL-20UF membranes (closed red circles *vs.* open blue circles in Fig. 3a and b, respectively). That is, even after the UCLs have undergone functionalization, and quantitatively contain less hydroxyl groups than their unfunctionalized CBL counterparts, there still appears to be a higher degree of electrostatic interactions between the diffusing MB molecules and UCLs in the hydrogels, as compared to those containing CBLs, regardless of lignin functionalization.

To highlight the impact of D on the variability of these time-dependent MB concentration data, Fig. 3c shows the permeated MB concentration as a function of (normalized) time for PVA-lignin composite hydrogels containing 10 wt% unfunctionalized UCLs (closed green symbols) and unfunctionalized CBLs (open black symbols). From Fig. 3c, we observe a significantly higher scatter in the MB permeation data between experiments for composite hydrogels fabricated from unfunctionalized CBLs when compared to those fabricated from unfunctionalized

UCLs. We believe this scatter in the permeation data alludes to the possibility that the higher D in heterogeneous CBLs results in the fabrication of membranes with more heterogeneous network structures, leading to higher scatter (or variation) in the transport properties extracted from the permeation experiments performed on these membranes. Note, we would like to point out to the reader that acrylate-based networks are inherently heterogeneous,^{122–124} so the lower dispersity of the UCLs may not be the only factor to consider when examining the final heterogeneity of the network structure. However, as seen from Fig. 3c, even when both samples are fabricated *via* the formation of arylate-based networks, the spread in the experimental permeation data between individual experiments is greater for CBL-based networks, as compared to those fabricated with UCLs. While additional experiments are needed to fully validate these claims, this result underscores the potential importance of utilizing well-defined, fractionated lignins of prescribed MWs, as these materials may provide a more robust platform to help elucidate the structure-processing-property relationships in this emerging class of green hydrogels. A quantitative description regarding the impact of the UCL and CBL on the network structure of the composite hydrogels will be presented and discussed later in this section.

Fig. 3d shows the MB permeability calculated (using eqn (1) in the Experimental section) for the PVA-lignin composite hydrogels containing both unfunctionalized and functionalized UCLs and CBLs. Note, as there was an initial lag time in the permeability data before any MB was detected in the receiving cell for PVA-lignin hydrogels, the permeability is extracted from the slope of the data post lag time. That is, the initial lag time was subtracted from the permeability data before the MB permeability was calculated. While this manipulation of the data does not alter the slope of the MB permeability data, the MB permeability calculated (and reported in Fig. 3d) does not necessarily represent a 'true' permeability, as there is an initial period of time where the diffusing MB molecules electrostatically interact with the accessible hydroxyl groups within the composite hydrogel until 'saturation' occurs, after which, unassociated MB molecules are allowed to permeate due to the concentration gradient across the membrane. However, we believe the MB permeabilities calculated herein serve as an 'effective' MB permeability, and as such, provide insight into how the introduction of lignins, both UCLs and CBLs, alters the permselectivity of the resulting composite membranes.

As seen in Fig. 3d, the concentration, type, and functionalization of the lignin affected the permeability of MB through the composite hydrogels. The MB permeability for the control membrane (that is, neat PVA) was approximately $5 \times 10^{-10} \text{ cm}^2 \text{ s}^{-1}$. Focusing on PVA-lignin composites containing UCLs, we observe that the introduction of 10 wt% UCLs results in an approximately 60% reduction in the permeability of MB through the membrane, regardless if the UCLs were functionalized ($5 \times 10^{-10} \text{ cm}^2 \text{ s}^{-1}$ *vs.* $2 \times 10^{-10} \text{ cm}^2 \text{ s}^{-1}$). We observe a more significant decrease in the MB permeability when the concentration of UCLs is increased to 20 wt%. As seen in Fig. 3d, the introduction of 20 wt% unfunctionalized UCLs resulted in almost a two orders of magnitude reduction in MB

permeability. However, while still significant, only an order of magnitude reduction in MB permeability was observed for composite membranes fabricated with functionalized UCLs.

Focusing our attention on PVA–CBL composites hydrogels in Fig. 3d, we see a similar qualitative behavior for the change in MB permeability with various concentrations of unfunctionalized and functionalized CBLs. With the introduction of 10 wt% CBLs (both unfunctionalized and functionalized), we see a similar reduction in MB permeability as was seen with membranes containing 10 wt% UCLs. That is, with the introduction of 10 wt% CBLs, the MB permeability dropped from a value of approximately $5 \times 10^{-10} \text{ cm}^2 \text{ s}^{-1}$ to approximately $2 \times 10^{-10} \text{ cm}^2 \text{ s}^{-1}$. However, unlike PVA–UCL–20UF membranes, only an order of magnitude reduction in MB permeability was observed with the introduction of 20 wt% unfunctionalized CBLs. Composite hydrogels containing 20 wt% functionalized UCLs and CBLs exhibited similar MB permeabilities ($\sim 3 \times 10^{-11} \text{ cm}^2 \text{ s}^{-1}$). With regards to MB permeability, PVA–UCL–20UF membranes exhibited both the longest initial time lag before MB was detectable in the receiving reservoir (see Fig. 3a), as well as the lowest ‘effective’ MB permeability (see Fig. 3d) of all the membranes investigated.

2.3. Young's modulus and equilibrium water uptake

Next, the mechanical (*i.e.*, Young's modulus) and hydration (*i.e.*, equilibrium water uptake) properties of the composite hydrogels were investigated. The Young's moduli and equilibrium water uptake of the hydrogels were measured, and the results of these measurements are summarized in Fig. 4a and b, respectively. Note, here the phrase “hydrated Young's modulus” refers to the Young's modulus of the hydrogels after the membranes were equilibrated in liquid water for at least 48 hours prior to the measurement. As seen in Fig. 4a, the Young's modulus of

hydrated neat PVA was approximately 8.5 MPa. Focusing our attention on PVA–UCL composite hydrogels, we observe that, at 10 wt% and 20 wt% lignin concentrations, and independent of lignin functionalization, the stiffnesses of these membranes are consistently lower than that of neat PVA, ranging in reductions of $\sim 5\%$ to $\sim 25\%$, for PVA–UCL–10F and PVA–UCL–10UF membranes, respectively. An increase in Young's modulus is finally observed when the UCL content was increased to 50 wt% (*i.e.*, PVA–UCL–50UF), where a $\sim 70\%$ greater modulus than that of neat PVA was measured. In contrast, the stiffnesses of the PVA–CBL membranes, at all concentrations and independent of lignin functionalization, are consistently higher than that of neat PVA, ranging in increases of $\sim 10\%$ to $\sim 40\%$, for PVA–CBL–20F and PVA–CBL–10F membranes, respectively. Following this same trend, PVA–CBL–50UF membranes exhibited a higher hydrated Young's modulus, $\sim 40\%$ higher than that of neat PVA. For the most part, we believe that the higher stiffnesses exhibited by membranes containing CBLs *vs.* those containing UCLs is primarily due to the higher apparent MW of the CBLs as compared to UCLs (1250 g mol^{-1} *vs.* 4170 g mol^{-1} for UCLs and CBLs, respectively). However, as mentioned above, we measured the highest Young's modulus for PVA–UCL–50UF membranes, so it appears that more than just the absolute MW of the lignins is playing a role in the observed moduli for hydrogels containing 50 wt% lignins, potentially related to the lower dispersity of the UCLs. Finally, we see that the stiffness of PVA–CBL membranes initially decreases when the lignin content is increased from 10 wt% to 20 wt%, but then increases again when the lignin content is further increased to 50 wt%. In conjunction with the permeability results shown in Fig. 3b, these results highlight how both the mechanical and transport properties of these composite membranes can be tuned, yielding both soft and stiff membranes with significantly reduced permeation of MB.

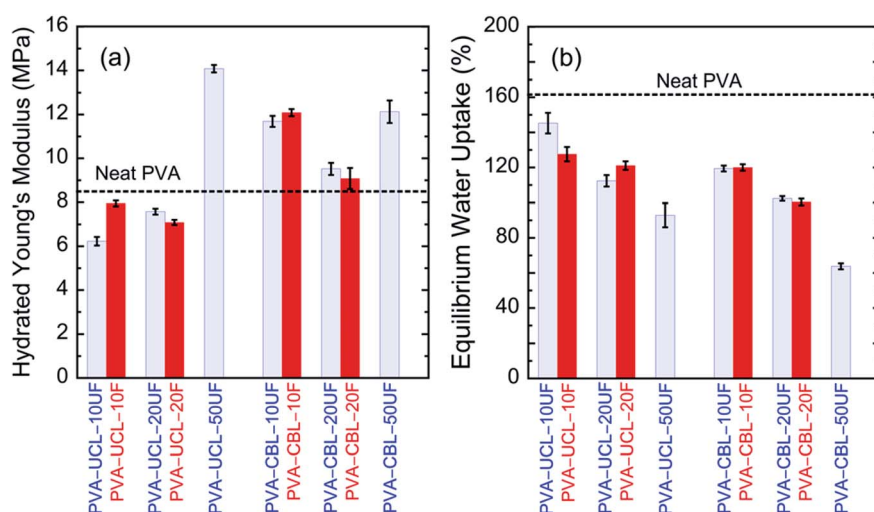


Fig. 4 (a) Hydrated Young's modulus (that is, Young's modulus of the hydrogel equilibrated in liquid water) and (b) equilibrium liquid water uptake of neat PVA and PVA–lignin composite membranes containing various concentrations of unfunctionalized (light blue bars) and functionalized (solid red bars) UCLs and CBLs. The dashed black lines in (a) and (b) represent the average hydrated Young's modulus and equilibrium water uptake of neat (or pristine) PVA (*i.e.*, PVA containing no lignin), respectively. Prior to both measurements, all hydrogels were hydrated in liquid water for at least 48 hours. Note, the error bars in the figures represent the standard deviation of (at least three) repeat experiments.

The reduction in Young's modulus with the addition of UCLs is even more surprising when we look at the equilibrium liquid water uptake values for these membranes. As seen in Fig. 4b, the water uptake percentages for PVA–lignin membranes containing UCLs range from $\sim 95\%$ to $\sim 145\%$ for PVA–UCL–50UF and PVA–UCL–10UF membranes, respectively. Note, water uptake for neat PVA is $\sim 160\%$. For the most part, the introduction of UCLs results in a decrease in the equilibrium water uptake in the composite membrane. Even with this reduction in equilibrium water uptake, composite membranes containing 10 wt% and 20 wt% UCLs are softer than neat PVA. In line with the highest hydrated Young's modulus measured for PVA–UCL–50UF, these membranes exhibited the highest reduction in equilibrium water uptake of all composites containing UCLs. Similarly, the introduction of CBLs to the PVA membrane results in a decrease in the equilibrium liquid water uptake of the resulting composite membranes. Specifically, the water uptakes ranged from $\sim 65\%$ to 120% for the PVA–CBL–50UF and PVA–CBL–10F membranes, respectively. As the hydrated stiffness of these membranes, in some cases, increased by $\sim 50\%$, it is not surprising that the equilibrium water uptake in these membranes is less than that of neat PVA. However, we must note that even when the equilibrium water uptake values between UCL and CBL membranes were similar, these membranes exhibited drastically different Young's moduli. For example, comparing PVA–UCL–10F to PVA–CBL–10F, we observe that the water uptake values for these membranes are $\sim 120\%$, though there is almost a 50% increase in Young's modulus when the UCLs are replaced by the CBLs. This result underscores that the introduction of UCLs and CBLs into the hydrogel is resulting in drastically different effects on the formation of the corresponding network structure.

2.4. Network structure of the composite hydrogels

To gain insight into how the introduction of lignin changes the network structure of the composite hydrogels, the molecular weight between crosslinks, M_c , was calculated for each membrane. The results of this analysis are shown in Fig. 5. Note, the dashed black line in Fig. 5 represents the average M_c of neat PVA (*i.e.*, PVA containing no lignin), which was calculated to be $\approx 800 \text{ g mol}^{-1}$. As seen in Fig. 5, the M_c of the composite hydrogels varies drastically with increasing lignin concentration, and for hydrogels containing UCLs, is seen to depend on whether the composite hydrogels contained functionalized UCLs. In general, the M_c is seen to decrease as the lignin content is increased from 10 wt% to 50 wt%. Most notably, PVA–UCL–20UF, PVA–UCL–50UF, both PVA–CBL–20UF and PVA–CBL–20F, and PVA–CBL–50UF membranes all exhibit similar values of M_c ($\approx 400 \text{ g mol}^{-1}$), which is $\approx 50\%$ lower than that of neat PVA. Interestingly, for composites containing CBLs, the calculated M_c does not change appreciably once the lignin content reaches 20 wt%, regardless of whether the lignin has undergone functionalization. We also observe that the functionalization of the UCL has a significant effect on the M_c , where this value is seen to decrease with increasing unfunctionalized UCL content. For composite hydrogels containing

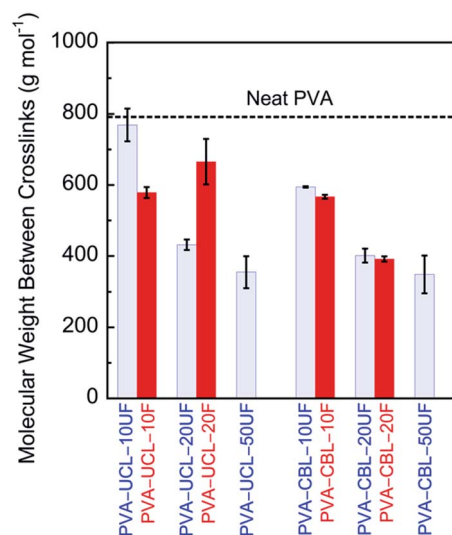


Fig. 5 The molecular weight between crosslinks, M_c , of pristine PVA and PVA–lignin composite membranes containing various concentrations of unfunctionalized (light blue bars) and functionalized (solid red bars) UCLs and CBLs. The dashed black line represents the average M_c of neat (or pristine) PVA (*i.e.*, PVA containing no lignin). Note, the error bars in the figure represent the standard deviation of (at least three) repeat experiments.

functionalized UCLs, the M_c for PVA–UCL–10F and PVA–UCL–20F are similar, where the average M_c is seen to increase from $\approx 600 \text{ g mol}^{-1}$ to $\approx 650 \text{ g mol}^{-1}$ when the concentration of functionalized UCL is doubled. In contrast, the average M_c is seen to decrease from $\approx 770 \text{ g mol}^{-1}$ to $\approx 400 \text{ g mol}^{-1}$ when the concentration of unfunctionalized UCL is doubled, though as mentioned previously, the calculated M_c does not change appreciably when the concentration of unfunctionalized UCL is increased from 20 wt% to 50 wt%.

In general, the observed changes in the M_c between the various composite hydrogels correlate with the observed reductions in MB permeabilities shown in Fig. 3d. First, with the exception of PVA–UCL–10UF, the calculated M_c for the composite hydrogels are lower than that of neat PVA, where, as seen in Fig. 3d, all composite hydrogels containing lignins exhibited lower MB permeabilities. Second, with the exception

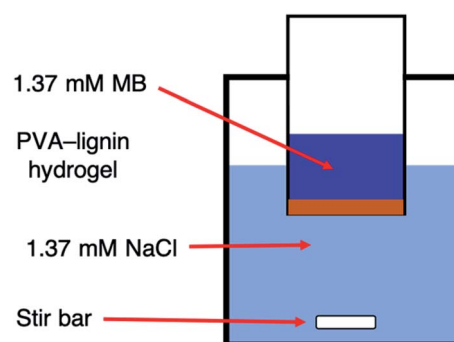


Fig. 6 Illustrative schematic of permeation cell used for methylene blue (MB) permeation experiments.

of PVA-UCL-20F, lower values of M_c were calculated for hydrogels containing 20 wt% UCLs and 20 wt% CBLs than those calculated for their 10 wt% counterparts, where lower MB permeabilities were observed for composite membranes containing 20 wt% UCLs and CBLs. However, the trends in the MB permeability data cannot be completely correlated to changes in the M_c between samples, as little change in the average M_c is observed when the lignin content was increased to 50 wt%, even though no MB was seen to permeate across hydrogels containing 50 wt% lignins. This result supports the notion that transport of MB molecules is governed by a combination of electrostatic interactions between the charged MB molecules and the lignin inside the composite hydrogels. However, in general, composite hydrogels containing 50 wt% lignin exhibited the highest Young's modulus and lowest equilibrium water uptake, which correlates well with the low values of M_c calculated for these membranes. Note, while these initial calculations of M_c obtained through swelling measurements provides a 'rough' picture of how the network structure changes with lignin content, obtaining independent calculations of the effective mesh size *via* mechanical indentation and neutron scattering is ongoing and is the focus of our future work.

3. Conclusion

In conclusion, we have synthesized free-standing PVA-lignin composite hydrogels containing various concentrations of unfunctionalized and functionalized UCLs and CBLs, where 'proof-of-concept' membranes containing as high as 50 wt% unfunctionalized lignins were fabricated. Successful functionalization of the lignins with vinyl-containing acrylate groups was confirmed by a combination of ^1H and ^{31}P NMR spectroscopy, where a higher reactivity of the $-\text{OH}$ groups in the fractionated UCLs was quantitatively observed. All composite hydrogels were shown to exhibit superior MB separation performance when compared to neat PVA. Additionally, an initial breakthrough time in the permeation data was observed for all composite hydrogels, which was attributed to the electrostatic interactions of the diffusing MB with the lignin inside the composite hydrogels. The length of this breakthrough time was seen to be a function of both the functionalization and type of lignin from which the composite membranes were fabricated. Longer initial breakthrough times were observed for membranes containing 20 wt% lignin, where the longest breakthrough time was observed for PVA-UCL-20UF membranes ($\sim 4 \times 10^7 \text{ s cm}^{-2}$). In contrast, the shortest breakthrough time was observed for composite membranes containing 10 wt% lignin ($\sim 1 \times 10^7 \text{ s cm}^{-2}$), both for membranes containing UCLs and CBLs and irrespective of functionalization. Notably, for permeation experiments for composite hydrogels containing 50 wt% unfunctionalized lignins, no MB was ever detected in the receiving reservoir, indicating that all of the MB in the donating reservoir was adsorbed by the composite hydrogel.

While all composite membranes exhibited significantly reduced MB permeability when compared with neat PVA, an over two order of magnitude reduction in MB permeability was observed for PVA-UCL-20UF membranes ($\sim 5 \times 10^{-10} \text{ cm}^2 \text{ s}^{-1}$ vs. $\sim 2 \times 10^{-12} \text{ cm}^2 \text{ s}^{-1}$). The Young's moduli of the composite

hydrogels fabricated with UCLs were consistently lower than that of the neat PVA. However, when the lignin concentration was increased to 50 wt% (PVA-UCL-50UF), a 70% increase in Young's modulus was observed. In contrast, the Young's moduli for membranes containing CBLs were consistently higher than that of the neat PVA hydrogels (over 50% in some cases). In general, the equilibrium liquid water uptake values of the composite membranes were consistently lower than that of neat PVA. Notably, the equilibrium water uptake of the neat PVA ($\sim 160\%$) was most significantly suppressed for PVA-CBL-50UF membranes ($\sim 64\%$). Finally, the concentration and functionalization of the lignins was seen to have a direct impact on the network structure of the soft composites, where in general, the molecular weight between crosslinks is seen to decrease with increasing lignin concentration. Results from this work highlight how lignin MW, dispersity, and functionality can be used to fabricate composite hydrogels that span a broad landscape of mechanical and transport properties. Furthermore, results from this work underscore the importance of utilizing well-defined (*i.e.*, low \bar{D}) lignins in the fabrication of these hydrogels, as they allow for a direct, systematic approach to elucidating the structure-processing-property relationships in this emerging class of green composite materials.

4. Experimental section

4.1. Material

Dimethyl sulfoxide (DMSO) (ACS reagent, $\geq 99.9\%$), dimethylformamide (DMF) (anhydrous, 99.8%), diethyl ether (ACS reagent, $\geq 98.0\%$, contains $\sim 2\%$ ethanol and ~ 10 ppm BHT as inhibitor), ammonium persulfate (APS) (ACS Reagent, $\geq 98.0\%$), methylenebisacrylamide (MBA) (99%), N,N,N',N' -tetramethylethylenediamine (TMEDA) (ReagentPlus®, 99%), acryloyl chloride (97.0%, contains < 210 ppm MEHQ as stabilizer), triethylamine ($\geq 99\%$), DMSO- d_6 (99.9 atom %D, contains 0.03% (v/v) TMS) were purchased from Sigma Aldrich. Methylene blue (MB) was purchased from VWR Analytical. Poly(vinyl alcohol) (MW = $78\,000 \text{ g mol}^{-1}$, 99 + % hydrolyzed) (PVA) was purchased from Polysciences, Inc. Kraft lignins ($M_N \approx 4170 \text{ g mol}^{-1}$, $\bar{D} \approx 3.9$), produced from the Sequential Liquid Lignin Recovery and Purification (SLRP) process,¹²⁵ were obtained from Liquid Lignin, LLC. From these Kraft lignins, ultraclean lignins ($M_N \approx 1250 \text{ g mol}^{-1}$, $\bar{D} \approx 2.2$), were produced from the Aqueous Lignin Purification with Hot Agents (ALPHA) process,⁴⁵ developed by the Thies Group at Clemson University. Briefly, the UCLs were isolated from the CBLs using a 50/50 (by volume) acetic acid–water solution at 70°C , with the low MW lignin of interest being isolated in the solvent-rich phase. The UCL was then precipitated from the solvent-rich phase as a solid by adding deionized (DI) water in a 1 : 1 (v/v) ratio. Reverse osmosis (RO) water (resistivity $\approx 18 \text{ M}\Omega \text{ cm}$) was used for all experiments.

4.2. Characterization of molecular weight of lignins

The molecular weight of the unfunctionalized UCLs and CBLs was determined using gel permeation chromatography (GPC). Specifically, the lignins were analyzed using an Alliance GPCV

2000 instrument. Two columns were used in series: (1) a Waters Styragel HT5 column (10 μm , 4.6 mm \times 300 mm) and (2) an Agilent PolarGel-L column (8 μm , 7.5 mm \times 300 mm). In this case, the mobile phase consisted of 0.05 mol L⁻¹ lithium bromide in DMF at a flow rate of 1 mL min⁻¹. Poly(ethylene glycol) (PEG) calibration standards were used for the estimation of the apparent molecular weight of the lignins. Samples were dissolved in the mobile phase at a concentration of 1 mg mL⁻¹ and were filtered using a 0.2 μm nylon membrane syringe filter prior to injection into the column. Detection of the PEG standards was carried out *via* a Waters differential refractometer, while the detection of lignins was carried out *via* ultraviolet-visible light (UV-vis) with a Waters 2487 detector at 280 nm.¹²⁶ The molecular weight for a given sample were generally reproducible within ± 50 g mol⁻¹.³⁸

4.3. Lignin acrylation procedure

After the aforementioned drying procedure, for example, 1 g of ultraclean lignin was immediately added to 5 mL of DMF in a RBF, and the solution was brought into a nitrogen atmosphere (*i.e.*, nitrogen glove box). Based on a previously developed method,¹²⁷ 786 μL of triethylamine, followed by 986 μL of acryloyl chloride, were added to the solution. The RBF was then capped with a rubber stopper and removed from the glove box. Next, the solution was left to stir for 24 h, after which it was vacuum filtered to remove unwanted salts. Precipitation and dissolution were performed three times using diethyl ether and DMF. This solution was then placed into a vacuum oven at room temperature under dynamic vacuum until all DMF was removed.

4.4. Characterization of lignins using infrared spectroscopy

Successful functionalization of the lignins was analyzed by FTIR spectroscopy using a Thermo Scientific Nicolet iS50R FT-IR equipped with Specac Golden Gate attenuated total reflectance (ATR) attachment. All spectra were collected using a liquid nitrogen-cooled mercury-cadmium-telluride detector with 64 scans per spectrum at a resolution of 4 cm⁻¹.

4.5. Lignin hydrogel synthesis

1 Thermally-crosslinked hydrogels. A solution of PVA and DMSO was produced by dissolving PVA in DMSO at 9% w/w for 6 h at 120 °C. After cooling to room temperature, high-purity nitrogen gas was bubbled through the PVA-DMSO solution for 1 h at room temperature. Additionally, pure DMSO was placed in a separate round bottom flask (RBF), and high-purity nitrogen gas was bubbled through the DMSO for 1 h at room temperature. The lignins (both crude bulk and ultraclean lignins) were dried in a room temperature oven under dynamic vacuum for 24 h. Note, to prevent thermal crosslinking of the lignins prior to their use in the fabrication procedure, the lignins were not dried at elevated temperatures (*i.e.*, were not dried above 60 °C). After drying, a prescribed amount of lignin (unfunctionalized or functionalized – see next section) was added to the purged DMSO and mixed until the lignin was fully dissolved, creating a dark black solution. The lignin-DMSO solution was then added to the PVA-DMSO solution, creating PVA-lignin-DMSO solutions at various lignin loadings

(10 wt%, 20 wt%, and 50 wt%, relative to the mass of PVA) and was stirred for 10 min to ensure homogeneous mixing of the two solutions. After 10 min of stirring, the solution was cast onto a polytetrafluoroethylene (PTFE) dish and placed into an oven under partial static vacuum at 60 °C for 36 hours or until all DMSO was removed, creating a robust, free-standing film. To remove any residual DMSO, the hydrogels were subjected to multiple Rinse-Soak cycles with DI water.

2 Thermally- and chemically-crosslinked hydrogels. For these composite hydrogels, everything in the aforementioned fabrication process remains the same except that we start with functionalized lignins (both UCLs and CBLs). Next, 1.5 wt% APS (relative to the mass of PVA) was dissolved in purged DMSO (<1 g) and added to the PVA-lignin-DMSO solution. After 1 min of stirring, 0.5 wt% MBA (relative to the mass of PVA) was dissolved in purged DMSO (<1 g) and added to the PVA-lignin-DMSO solution. After 1 min of stirring, 0.75 wt% TMEDA (relative to the mass of PVA) was added to the PVA-lignin-DMSO solution. After 5 min of stirring, the solution was cast onto a polytetrafluoroethylene (PTFE) dish and placed into an oven under partial static vacuum at 60 °C for 36 hours or until all DMSO was removed, creating a robust, free-standing film. To remove any residual DMSO, the hydrogels were subjected to multiple Rinse-Soak cycles with DI water. Once fabricated, all composite hydrogels were stored in DI water at room temperature (~20 °C) until they were used in experiments.

4.6. Mechanical indentation experiments

Hydrated Young's modulus measurements, based on the JKR (Johnson-Kendall-Roberts) theory of adhesion,¹²⁸ were conducted using a custom-built mechanical indentation apparatus. The setup consisted of a high-resolution linear actuator (M-230.25, Physike Instrumente) and mercury servo controller (C-863.11, Physike Instrumente) connected to a S-beam load cell (Futek LSB200, FUTEK Advanced Sensor Technology, Inc) with a rigid glass indenter of radius of curvature $R = 3.308$ mm. The linear actuator was mounted to a high-performance linear stage with 46 mm of travel range (M433, Newport). A custom program designed in LabVIEW was used to acquire load and indenter height data as a function of time from the S-beam load cell and the linear actuator, respectively, during all indentation experiments. For these experiments, the indenter was lowered at a speed of 2 $\mu\text{m s}^{-1}$ until the indenter came in contact with the swollen hydrogel. Upon contact, the indenter velocity increased to 4 $\mu\text{m s}^{-1}$ until a prescribed load of 29.4 mN was reached, after which the indenter was retracted from the sample. Using Hertz's solution for spherical indentation, a solution to Hooke's law was used to acquire Young's modulus.¹²⁹ Note, prior to beginning all indentation experiments, the membranes were equilibrated in liquid water for at least 48 h. Also, the Poisson's ratio (ν) of the hydrated composite hydrogels was assumed to be $\nu = 0.5$.

4.7. Nuclear magnetic resonance spectroscopy

Characterization of the lignins, before and after acrylation, was performed using ¹H nuclear magnetic resonance (NMR) spectroscopy on a Bruker 300 MHz. The lignin was dissolved in DMSO-

d_6 at a concentration of $\sim 4 \text{ mg mL}^{-1}$ and placed into an NMR tube. Measurements were performed at 16 scans per spectrum. All spectra were Fourier-transformed, baseline corrected, and phased using SpinWorks. Of interest to this investigation were NMR peaks corresponding to the aromatic ($\delta = 6.7 \text{ ppm}$) and aliphatic ($\delta = 3.7 \text{ ppm}$) hydroxyl ($-\text{OH}$) groups,¹³⁰ as well as the peak corresponding to protons on a vinyl group ($\delta = 6.2 \text{ ppm}$).¹³¹

Additional characterization of the hydroxyl content of the lignins, before and after acrylation, was performed using ^{31}P NMR spectroscopy on a Bruker Neo 500 MHz (with cryoprobe). The solutions for dissolving lignin were prepared from the following: (1) 1 mL of chloroform- d and 1.6 mL of pyridine, and (2) 1 mL of chloroform- d , 1.6 mL of pyridine, 100 mg of cyclohexanol (internal standard), and 90 mg of chromium acetylacetonate. 20 mg of vacuum dried lignin were added to a solution containing 400 μL of (1) and 150 μL of (2). 50 μL of 2-chloro-4,4,5,5-tetramethyl-1,3,2-dioxaphospholane (TMDP) was added to this solution and transferred into an NMR tube. Measurements were performed within 30 minutes of sample prep and at 32 scans/spectrum. All spectra were Fourier-transformed, baseline corrected, and phased using TopSpin. Of interest to this investigation were NMR peaks corresponding to the aromatic ($\delta = 144.6\text{--}137.3 \text{ ppm}$) and aliphatic ($\delta = 149.1\text{--}145.4 \text{ ppm}$) hydroxyl ($-\text{OH}$) groups.¹¹⁷

4.8. Methylene blue permeation

A custom-built diffusion cell was used for MB permeation experiments. As depicted in Fig. 6, the hydrated hydrogel was sandwiched between a receiving reservoir filled with 25 mL of 1.37 mmol L^{-1} NaCl in RO water and a donating reservoir filled with 2 mL of 1.37 mmol L^{-1} MB in RO water. To measure the concentration of MB in the receiving reservoir, aliquots were taken at fixed time intervals. The concentration of MB ions in each aliquot was measured *via* ultraviolet-visible light (UV-vis) spectroscopy (VWR, UV-3100PV), scanning from wavelengths of 700 nm to 600 nm. Following the scan, the aliquot was immediately returned to the receiving reservoir. Observed in the UV-vis spectrum, the prominent peak at 662 nm is attributed to MB ions.¹³² From these data, the permeability of MB ions can be calculated from the following equation:¹³³

$$V_R \frac{dC_R(t)}{dt} = A \frac{P}{L} C_D \quad (1)$$

where C_D and $C_R(t)$ are the MB ion concentrations (mol L^{-1}) in the donating and receiving reservoirs, respectively, A and L are the area (cm^2) and thickness (cm) of the membrane, respectively, P is the permeability of MB ions ($\text{cm}^2 \text{ s}^{-1}$), and V_R is the volume (L) of the receiving cell. The following assumptions were made in use of this expression: (1) MB permeability is independent of ion concentration; (2) permeation in the membrane is at pseudo-steady state; and (3) the concentration of MB in the donating reservoir remains constant and $C_D \gg C_R(t)$.

4.9. Equilibrium liquid water uptake

The equilibrium liquid water uptake of the membranes was determined for each hydrogel by first immersing the hydrogel in RO water for at least 48 h. After 48 h, the hydrogels were

removed from the RO water, quickly patted with a KimWipe to remove any liquid water on the membrane surface, and then weighed using an analytical balance (Mettler Toledo ME204E) to obtain the hydrated mass of the hydrogel. To measure the dry weight, the hydrogels were dried at 90°C for 24 h under dynamic vacuum. After 24 h, the membranes were removed from the oven and quickly weighed using an analytical balance. The equilibrium liquid water uptake for each membrane was calculated using the following equation:

$$\text{Water uptake} = \left(\frac{W_{\text{wet}} - W_{\text{dry}}}{W_{\text{dry}}} \right) \times 100\% \quad (2)$$

where W_{wet} and W_{dry} are the hydrated and dry mass of the hydrogel, respectively.

4.10. Characterization of molecular weight between crosslinks

The molecular weight between crosslinks of the membranes was calculated based on the Peppas-Merrill equation.¹³⁴ The swollen, wet mass of the membranes was determined by first immersing the hydrogel in RO water for at least 48 h. After 48 h, the hydrogels were removed from the RO water, quickly patted with a KimWipe to remove any liquid water on the membrane surface, and then weighed using an analytical balance (Mettler Toledo ME204E) to obtain the hydrated (swollen) mass of the hydrogel. To weigh the hydrogel in the relaxed state, the hydrogels were dried at 60°C for 3.75 h under 10 inHg vacuum. After 3.75 h, the hydrogels were quickly weighed to acquire a relaxed membrane mass. Note, due to the fact that the hydrogels were fabricated in DMSO, and not water, this step of the procedure is slightly different than the traditional method reported in literature. The hydrogels were then put back into the oven at 100°C for 24 h under dynamic vacuum to acquire a mass in the dried state. The following equations were then used to acquire the polymer volume fractions in the swollen ($v_{2,s}$) and relaxed ($v_{2,r}$) state:¹³⁵

$$Q = \left(\frac{W_{\text{wet}} - W_{\text{dry}}}{W_{\text{dry}}} \right) \quad (3)$$

$$v_{2,s} = \frac{1}{Q \frac{\rho}{\rho_{\text{H}_2\text{O}}} + 1} \quad (4)$$

where Q is the mass swelling ratio, ρ is polymer density, and $\rho_{\text{H}_2\text{O}}$ is the density of water. These values were then used in the following Peppas-Merrill equation:

$$\frac{1}{M_c} = \frac{1}{M_n} - \frac{1}{V_1} \frac{[\ln(1 - v_{2,s}) + v_{2,s} + \chi v_{2,s}^2]}{\rho v_{2,r} \left[\left(\frac{v_{2,s}}{v_{2,r}} \right)^{\frac{1}{3}} - \frac{1}{2} \left(\frac{v_{2,s}}{v_{2,r}} \right) \right]} \quad (5)$$

where M_n is the number average molecular weight of the polymer, χ is the Flory-Huggins parameter and was taken from previous work on PVA-water systems,¹³⁶ and V_1 is the molar volume of water ($\approx 18 \text{ cm}^3$).

Conflicts of interest

The authors declare no competing financial interest.

Acknowledgements

This material is based upon work supported by the National Science Foundation under Grant No. CBET-1915787 and CBET-1403873. This work utilized a 500 MHz NEO NMR spectrometer with cryoprobe that was purchased through the NSF Major Research Instrumentation (MRI) Program, Grant No. CHE-1725919. Nicholas Gregorich would like to acknowledge of the support of the Department of Education Graduate Assistance in Areas of National Need (GAANN) Fellowship Program (P200A180076). The authors would also like to thank Dr Jaime Idarraga-Mora for all his help with the development and installation of a LabView program to control the mechanical indentation apparatus.

References

- 1 K. Rohrbach, Y. Li, H. Zhu, Z. Liu, J. Dai, J. Andreasen and L. Hu, *Chem. Commun.*, 2014, **50**, 13296–13299.
- 2 Y. Gao, R. Guo, Y. Feng, L. Zhang, C. Wang, J. Song, T. Jiao, J. Zhou and Q. Peng, *ACS Omega*, 2018, **3**, 11663–11672.
- 3 J. Domínguez-Robles, M. S. Peresin, T. Tamminen, A. Rodríguez, E. Larrañeta and A.-S. Jääskeläinen, *Int. J. Biol. Macromol.*, 2018, **115**, 1249–1259.
- 4 Y. Zhu, Y. Zheng, F. Wang and A. Wang, *Chem. Eng. J.*, 2016, **284**, 422–430.
- 5 N. Li and R. Bai, *Sep. Purif. Technol.*, 2005, **42**, 237–247.
- 6 X. Cheng, Y. Jin, T. Sun, R. Qi, B. Fan and H. Li, *RSC Adv.*, 2015, **5**, 4162–4170.
- 7 S. Mondal, C. Li and K. Wang, *J. Chem. Eng. Data*, 2015, **60**, 2356–2362.
- 8 S. A. Dergunov and G. A. Mun, *Radiat. Phys. Chem.*, 2009, **78**, 65–68.
- 9 A. Das, M. Mehndiratta, P. Chattopadhyay and A. R. Ray, *J. Appl. Polym. Sci.*, 2010, **115**, 393–403.
- 10 S. S. Vaghani and M. M. Patel, *Drug Dev. Ind. Pharm.*, 2011, **37**, 1160–1169.
- 11 A. Sannino, C. Demitri and M. Madaghiele, *Materials*, 2009, **2**, 353–373.
- 12 N. Peng, Y. Wang, Q. Ye, L. Liang, Y. An, Q. Li and C. Chang, *Carbohydr. Polym.*, 2016, **137**, 59–64.
- 13 V. K. Thakur and M. K. Thakur, *Int. J. Biol. Macromol.*, 2015, **72**, 834–847.
- 14 S. Thakur, P. P. Govender, M. A. Mamo, S. Tamulevicius, Y. K. Mishra and V. K. Thakur, *Vacuum*, 2017, **146**, 342–355.
- 15 E. Larrañeta, M. Imízcoz, J. X. Toh, N. J. Irwin, A. Ripolin, A. Perminova, J. Domínguez-Robles, A. Rodríguez and R. F. Donnelly, *ACS Sustainable Chem. Eng.*, 2018, **6**, 9037–9046.
- 16 K. Rajan, J. K. Mann, E. English, D. P. Harper, D. J. Carrier, T. G. Rials, N. Labbé and S. C. Chmely, *Biomacromolecules*, 2018, **19**, 2665–2672.
- 17 W. K. El-Zawawy and M. M. Ibrahim, *J. Appl. Polym. Sci.*, 2012, **124**, 4362–4370.
- 18 D. Ciolacu, A. M. Oprea, N. Anghel, G. Cazacu and M. Cazacu, *Mater. Sci. Eng. C*, 2012, **32**, 452–463.
- 19 D. Kai, Z. W. Low, S. S. Liow, A. Abdul Karim, H. Ye, G. Jin, K. Li and X. J. Loh, *ACS Sustainable Chem. Eng.*, 2015, **3**, 2160–2169.
- 20 X. You, X. Wang, H. J. Zhang, K. Cui, A. Zhang, L. Wang, C. Yadav and X. Li, *ACS Appl. Mater. Interfaces*, 2020, **12**, 39892–39901.
- 21 L. Cheng, B. Deng, W. Luo, S. Nie, X. Liu, Y. Yin, S. Liu, Z. Wu, P. Zhan, L. Zhang and J. Chen, *J. Agric. Food Chem.*, 2020, **68**, 5249–5258.
- 22 L. Dai, M. Ma, J. Xu, C. Si, X. Wang, Z. Liu and Y. Ni, *Chem. Mater.*, 2020, **32**, 4324–4330.
- 23 S. Chandna, N. S. Thakur, R. Kaur and J. Bhaumik, *Biomacromolecules*, 2020, **21**, 3216–3230.
- 24 N. Tahari, P. L. de Hoyos-Martinez, M. Abderrabba, S. Ayadi and J. Labidi, *Colloids Surf., A*, 2020, **602**, 125108.
- 25 L. Zhang, H. Lu, J. Chu, J. Ma, Y. Fan, Z. Wang and Y. Ni, *ACS Sustainable Chem. Eng.*, 2020, **8**, 12655–12663.
- 26 J. Xu, J. J. Xu, Q. Lin, L. Jiang, D. Zhang, Z. Li, B. Ma, C. Zhang, L. Li, D. Kai, H.-D. Yu and X. J. Loh, *ACS Appl. Bio Mater.*, 2020, DOI: 10.1021/acsabm.0c00858.
- 27 R. C. Andeme Ela, M. Tajiri, N. K. Newberry, P. A. Heiden and R. G. Ong, *ACS Sustainable Chem. Eng.*, 2020, **8**, 17299–17306.
- 28 K. Crouvisier-Urien, P. R. Bodart, P. Winckler, J. Raya, R. D. Gougeon, P. Cayot, S. Domenek, F. Debeaufort and T. Karbowiak, *ACS Sustainable Chem. Eng.*, 2016, **4**, 6371–6381.
- 29 C. Pouteau, P. Dole, B. Cathala, L. Averous and N. Boquillon, *Polym. Degrad. Stab.*, 2003, **81**, 9–18.
- 30 X. Dong, M. Dong, Y. Lu, A. Turley, T. Jin and C. Wu, *Ind. Crops Prod.*, 2011, **34**, 1629–1634.
- 31 J. Sunthornvarabhas, S. Liengprayoon and T. Suwonsichon, *Ind. Crops Prod.*, 2017, **109**, 857–861.
- 32 M. Parit, P. Saha, V. A. Davis and Z. Jiang, *ACS Omega*, 2018, **3**, 10679–10691.
- 33 H. Sadeghifar, R. Venditti, J. Jur, R. E. Gorga and J. J. Pawlak, *ACS Sustainable Chem. Eng.*, 2017, **5**, 625–631.
- 34 D. Kai, M. J. Tan, P. L. Chee, Y. K. Chua, Y. L. Yap and X. J. Loh, *Green Chem.*, 2016, **18**, 1175–1200.
- 35 A. Duval and M. Lawoko, *React. Funct. Polym.*, 2014, **85**, 78–96.
- 36 S. Dutta, K. C.-W. Wu and B. Saha, *Catal. Sci. Technol.*, 2014, **4**, 3785–3799.
- 37 H. Wang, Y. Pu, A. Ragauskas and B. Yang, *Bioresour. Technol.*, 2019, **271**, 449–461.
- 38 A. S. Klett, A. M. Payne and M. C. Thies, *ACS Sustainable Chem. Eng.*, 2016, **4**, 6689–6694.
- 39 A. S. Klett, A. M. Payne, T. Phongpreecha, D. B. Hodge and M. C. Thies, *Ind. Eng. Chem. Res.*, 2017, **56**, 9778–9782.
- 40 V. K. Thakur and M. K. Thakur, *Int. J. Biol. Macromol.*, 2015, **72**, 834–847.
- 41 R. M. O'Dea, J. A. Willie and T. H. Epps, *ACS Macro Lett.*, 2020, 476–493.

- 42 M. S. Ganewatta, H. N. Lokupitiya and C. Tang, *Polymers*, 2019, **11**, 1176.
- 43 B. M. Upton and A. M. Kasko, *Chem. Rev.*, 2016, **116**, 2275–2306.
- 44 V. K. Thakur, M. K. Thakur, P. Raghavan and M. R. Kessler, *ACS Sustainable Chem. Eng.*, 2014, **2**, 1072–1092.
- 45 A. S. Klett, P. V. Chappell and M. C. Thies, *Chem. Commun.*, 2015, **51**, 12855–12858.
- 46 P. Asawaworarit, P. Daorattanachai, W. Laosiripojana, C. Sakdaronnarong, A. Shotipruk and N. Laosiripojana, *Chem. Eng. J.*, 2019, **356**, 461–471.
- 47 X. Zhang, Q. Zhang, J. Long, Y. Xu, T. Wang, L. Ma and Y. Li, *BioResources*, 2014, **9**, 3347–3360.
- 48 X. Liu, Z. Jiang, S. Feng, H. Zhang, J. Li and C. Hu, *Fuel*, 2019, **244**, 247–257.
- 49 Q. Liu, S. Wang, Y. Zheng, Z. Luo and K. Cen, *J. Anal. Appl. Pyrolysis*, 2008, **82**, 170–177.
- 50 H. Kawamoto, *J. Wood Sci.*, 2017, **63**, 117–132.
- 51 H. Yang, R. Yan, H. Chen, D. H. Lee and C. Zheng, *Fuel*, 2007, **86**, 1781–1788.
- 52 W. Qu, Y. Xue, Y. Gao, M. Rover and X. Bai, *Biomass Bioenergy*, 2016, **95**, 19–26.
- 53 Y. Xu, F. You, H. Sun and L. Shao, *ACS Sustainable Chem. Eng.*, 2017, **5**, 5520–5528.
- 54 S. Wang, L. Shuai, B. Saha, D. G. Vlachos and T. H. Epps, *ACS Cent. Sci.*, 2018, **4**, 701–708.
- 55 A. L. Holmberg, N. A. Nguyen, M. G. Karavolias, K. H. Reno, R. P. Wool and T. H. Epps, *Macromolecules*, 2016, **49**, 1286–1295.
- 56 T. Lindström, *Colloid Polym. Sci.*, 1979, **257**, 277–285.
- 57 T. Lindström and L. Westman, *Colloid Polym. Sci.*, 1980, **258**, 390–397.
- 58 T. Lindström and L. Westman, *Colloid Polym. Sci.*, 1982, **260**, 594–598.
- 59 E. Larrañeta, M. Imízcoz, J. X. Toh, N. J. Irwin, A. Ripolin, A. Perminova, J. Domínguez-Robles, A. Rodríguez and R. F. Donnelly, *ACS Sustainable Chem. Eng.*, 2018, **6**, 9037–9046.
- 60 D. Kai, Z. W. Low, S. S. Liow, A. Abdul Karim, H. Ye, G. Jin, K. Li and X. J. Loh, *ACS Sustainable Chem. Eng.*, 2015, **3**, 2160–2169.
- 61 F. Oveissi, S. Naficy, T. Y. L. Le, D. F. Fletcher and F. Dehghani, *ACS Appl. Bio Mater.*, 2018, **1**, 2073–2081.
- 62 K. Rajan, J. K. Mann, E. English, D. P. Harper, D. J. Carrier, T. G. Rials, N. Labbé and S. C. Chmely, *Biomacromolecules*, 2018, **19**, 2665–2672.
- 63 H. Liu and H. Chung, *J. Polym. Sci., Part A: Polym. Chem.*, 2017, **55**, 3515–3528.
- 64 H. Liu and H. Chung, *Macromolecules*, 2016, **49**, 7246–7256.
- 65 X. Shen, P. Berton, J. L. Shamshina and R. D. Rogers, *Green Chem.*, 2016, **18**, 5607–5620.
- 66 C. Jin, X. Zhang, J. Xin, G. Liu, G. Wu, Z. Kong and J. Zhang, *ACS Sustainable Chem. Eng.*, 2017, **5**, 4086–4093.
- 67 Y. Ge and Z. Li, *ACS Sustainable Chem. Eng.*, 2018, **6**, 7181–7192.
- 68 W. Xu, X. Wang, N. Sandler, S. Willför and C. Xu, *ACS Sustainable Chem. Eng.*, 2018, **6**, 5663–5680.
- 69 H. Zhang, W. Zhang, H. Ming, J. Pang, H. Zhang, G. Cao and Y. Yang, *Chem. Eng. J.*, 2018, **341**, 280–288.
- 70 L. Passauer, in *Functional Materials from Renewable Sources*, American Chemical Society, 2012, vol. 1107, pp. 211–228.
- 71 J. E. Peñaranda A. and M. A. Sabino, *Polym. Bull.*, 2010, **65**, 495–508.
- 72 W. E. Rudzinski, A. M. Dave, U. H. Vaishnav, S. G. Kumbar, A. R. Kulkarni and T. M. Aminabhavi, *Des. Monomers Polym.*, 2002, **5**, 39–65.
- 73 S. Park, S. H. Kim, J. H. Kim, H. Yu, H. J. Kim, Y.-H. Yang, H. Kim, Y. H. Kim, S. H. Ha and S. H. Lee, *J. Mol. Catal. B: Enzym.*, 2015, **119**, 33–39.
- 74 D. Ciolacu, A. M. Oprea, N. Anghel, G. Cazacu and M. Cazacu, *Mater. Sci. Eng. C*, 2012, **32**, 452–463.
- 75 T. Leskinen, J. Witos, J. J. Valle-Delgado, K. Lintinen, M. Kostianen, S. K. Wiedmer, M. Österberg and M.-L. Mattinen, *Biomacromolecules*, 2017, **18**, 2767–2776.
- 76 S. Sathawong, W. Sridach and K. Techato, *J. Environ. Chem. Eng.*, 2018, **6**, 5879–5888.
- 77 M. Fernández-Pérez, M. Villafranca-Sánchez, F. Flores-Céspedes and I. Daza-Fernández, *Carbohydr. Polym.*, 2011, **83**, 1672–1679.
- 78 J. Domínguez-Robles, M. S. Peresin, T. Tamminen, A. Rodríguez, E. Larrañeta and A.-S. Jääskeläinen, *Int. J. Biol. Macromol.*, 2018, **115**, 1249–1259.
- 79 C. Yu, F. Wang, C. Zhang, S. Fu and L. A. Lucia, *React. Funct. Polym.*, 2016, **106**, 137–142.
- 80 X. Wang, C. Jiang, B. Hou, Y. Wang, C. Hao and J. Wu, *Chemosphere*, 2018, **206**, 587–596.
- 81 J. A. Emerson, N. T. Garabedian, D. L. Burris, E. M. Furst and T. H. Epps, *ACS Sustainable Chem. Eng.*, 2018, **6**, 6856–6866.
- 82 J. Ding, A. S. Klett, J. A. Gamble, G. W. Tindall and M. C. Thies, *Fluid Phase Equilib.*, 2018, **461**, 8–14.
- 83 M. C. Thies, A. S. Klett and D. A. Bruce, *US Pat.*, US 10053482 B2, 2018.
- 84 L. L. Xia, C. L. Li and Y. Wang, *J. Membr. Sci.*, 2016, **498**, 263–275.
- 85 Y. Liu, L. M. Geever, J. E. Kennedy, C. L. Higginbotham, P. A. Cahill and G. B. McGuinness, *J. Mech. Behav. Biomed. Mater.*, 2010, **3**, 203–209.
- 86 H. S. Mansur, C. M. Sadahira, A. N. Souza and A. A. P. Mansur, *Mater. Sci. Eng. C*, 2008, **28**, 539–548.
- 87 H. S. Mansur, R. L. Oréfice and A. A. P. Mansur, *Polymer*, 2004, **45**, 7193–7202.
- 88 A. Hasimi, A. Stavropoulou, K. G. Papadokostaki and M. Sanopoulou, *Eur. Polym. J.*, 2008, **44**, 4098–4107.
- 89 Y. Wang and Y.-L. Hsieh, *J. Appl. Polym. Sci.*, 2010, **116**, 3249–3255.
- 90 J.-S. Park, J.-W. Park and E. Ruckenstein, *Polymer*, 2001, **42**, 4271–4280.
- 91 A. A. M. Alfayyadh, S. Lotfy, A. A. Basfar and M. I. Khalil, *Prog. Nat. Sci.: Mater. Int.*, 2017, **27**, 316–325.
- 92 K. C. S. Figueiredo, T. L. M. Alves and C. P. Borges, *J. Appl. Polym. Sci.*, 2009, **111**, 3074–3080.
- 93 C.-K. Yeom and K.-H. Lee, *J. Membr. Sci.*, 1996, **109**, 257–265.

- 94 S. A. Stone, P. Gosavi, T. J. Athauda and R. R. Ozer, *Mater. Lett.*, 2013, **112**, 32–35.
- 95 R. Shi, J. Bi, Z. Zhang, A. Zhu, D. Chen, X. Zhou, L. Zhang and W. Tian, *Carbohydr. Polym.*, 2008, **74**, 763–770.
- 96 S. Wang, J. Ren, W. Li, R. Sun and S. Liu, *Carbohydr. Polym.*, 2014, **103**, 94–99.
- 97 E. Rynkowska, K. Fatyeyava, S. Marais, J. Kujawa and W. Kujawski, *Polymers*, 2019, **11**, 1799.
- 98 C. M. Hassan and N. A. Peppas, *Macromolecules*, 2000, **33**, 2472–2479.
- 99 Y. Guo, J. Bae, Z. Fang, P. Li, F. Zhao and G. Yu, *Chem. Rev.*, 2020, **120**, 7642–7707.
- 100 N. Joshi, K. Suman and Y. M. Joshi, *Macromolecules*, 2020, **53**, 3452–3463.
- 101 J. Tavakoli, J. Gascooke, N. Xie, B. Z. Tang and Y. Tang, *ACS Appl. Polym. Mater.*, 2019, **1**, 1390–1398.
- 102 S. R. Stauffer and N. A. Peppas, *Polymer*, 1992, **33**, 3932–3936.
- 103 C. M. Hassan, J. E. Stewart and N. A. Peppas, *Eur. J. Pharm. Biopharm.*, 2000, **49**, 161–165.
- 104 Z. Lian and L. Ye, *J. Appl. Polym. Sci.*, 2013, **128**, 3325–3329.
- 105 A. S. Hickey and N. A. Peppas, *J. Membr. Sci.*, 1995, **107**, 229–237.
- 106 Y. Hou, C. Chen, K. Liu, Y. Tu, L. Zhang and Y. Li, *RSC Adv.*, 2015, **5**, 24023–24030.
- 107 M. A. Lake and J. C. Blackburn, *US Pat.*, US 9260464 B2, 2016.
- 108 W. Xiao, J. He, J. W. Nichol, L. Wang, C. B. Hutson, B. Wang, Y. Du, H. Fan and A. Khademhosseini, *Acta Biomater.*, 2011, **7**, 2384–2393.
- 109 S. J. Lee, S. S. Kim and Y. M. Lee, *Carbohydr. Polym.*, 2000, **41**, 197–205.
- 110 D. Myung, W. Koh, J. Ko, Y. Hu, M. Carrasco, J. Noolandi, C. N. Ta and C. W. Frank, *Polymer*, 2007, **48**, 5376–5387.
- 111 S. J. Kim, S. J. Park and S. I. Kim, *React. Funct. Polym.*, 2003, **55**, 53–59.
- 112 E. S. Dragan, *Chem. Eng. J.*, 2014, **243**, 572–590.
- 113 A. J. Silvaroli, T. R. Heyl, Z. Qiang, J. M. Beebe, D. Ahn, S. Mangold, K. R. Shull and M. Wang, *ACS Appl. Mater. Interfaces*, 2020, **12**, 44125–44136.
- 114 T. Nakajima, H. Furukawa, Y. Tanaka, T. Kurokawa, Y. Osada and J. P. Gong, *Macromolecules*, 2009, **42**, 2184–2189.
- 115 L. H. Sperling, in *Interpenetrating Polymer Networks*, ed. D. Klemperer, L. H. Sperling and L. A. Utracki, American Chemical Society, Washington, DC, 1994, vol. 239, pp. 3–38.
- 116 Y. Pu, S. Cao and A. J. Ragauskas, *Energy Environ. Sci.*, 2011, **4**, 3154.
- 117 S. Kalami, M. Arefmanesh, E. Master and M. Nejad, *J. Appl. Polym. Sci.*, 2017, **134**, 45124.
- 118 D. Argyropoulos, *J. Membr. Sci.*, 1994, **14**, 45–63.
- 119 R. Safou-Tchiam, T. A. Barhé, P. Soulounganga, A. G. Akagah and B. D. Jeso, *J. Mater. Environ. Sci.*, 2017, **8**, 2530–2540.
- 120 R. Milotskyi, L. Szabó, K. Takahashi and C. Bliard, *Front. Chem.*, 2019, **7**, 633.
- 121 P. Sannigrahi, Y. Pu and A. Ragauskas, *Curr. Opin. Environ. Sustain.*, 2010, **2**, 383–393.
- 122 A. F. Senyurt, H. Wei, C. E. Hoyle, S. G. Piland and T. E. Gould, *Macromolecules*, 2007, **40**, 4901–4909.
- 123 S. Ye, N. B. Cramer and C. N. Bowman, *Macromolecules*, 2011, **44**, 490–494.
- 124 B. H. Jones, T. M. Alam, S. Lee, M. C. Celina, J. P. Allers, S. Park, L. Chen, E. J. Martinez and J. L. Unangst, *Polymer*, 2020, **205**, 122783.
- 125 J. Velez and M. C. Thies, *J. Wood Chem. Technol.*, 2016, **36**, 27–41.
- 126 S. H. Ghaffar and M. Fan, *Biomass Bioenergy*, 2013, **57**, 264–279.
- 127 A. S. Sawhney, C. P. Pathak and J. A. Hubbell, *Macromolecules*, 1993, **26**, 581–587.
- 128 K. L. Johnson, K. Kendall and A. D. Roberts, *Proc. R. Soc. A*, 1971, **324**, 301–313.
- 129 M. Sakai and S. Shimizu, *J. Non-Cryst. Solids*, 2001, **282**, 236–247.
- 130 T. Rashid, C. F. Kait, I. Regupathi and T. Murugesan, *Ind. Crops Prod.*, 2016, **84**, 284–293.
- 131 K. Son and J. Lee, *Materials*, 2016, **9**, 854.
- 132 R. Zhao, Y. Wang, X. Li, B. Sun and C. Wang, *ACS Appl. Mater. Interfaces*, 2015, **7**, 26649–26657.
- 133 E. M. Davis, J. Kim, V. P. Oleshko, K. A. Page and C. L. Soles, *Adv. Funct. Mater.*, 2015, **25**, 4064–4075.
- 134 N. A. Peppas and E. W. Merrill, *J. Polym. Sci., Polym. Chem. Ed.*, 1976, **14**, 441–457.
- 135 A. Cavallo, M. Madaghiele, U. Masullo, M. G. Lionetto and A. Sannino, *J. Appl. Polym. Sci.*, 2017, **134**, 44380.
- 136 I. Sakurada, A. Nakajima and H. Fujiwara, *J. Polym. Sci.*, 1959, **35**, 497–505.